Real-Time Iterative Monitoring of Radiofrequency Ablation Tumor Therapy with ^{15}O-Water PET Imaging

Ande Bao[1,2], Beth Goins[1], Gerald D. Dodd III[1], Anuradha Soundararajan[1], Cristina Santoyo[1], Randal A. Otto[2], Michael D. Davis[3], and William T. Phillips[1]

[1]Department of Radiology, University of Texas Health Science Center at San Antonio, San Antonio, Texas; [2]Department of Otolaryngology–Head and Neck Surgery, University of Texas Health Science Center at San Antonio, San Antonio, Texas; and [3]Research Imaging Center, University of Texas Health Science Center at San Antonio, San Antonio, Texas

A method that provides real-time image-based monitoring of solid tumor therapy to ensure complete tumor eradication during image-guided interventional therapy would be a valuable tool. The short, 2-min half-life of ^{15}O makes it possible to perform repeated PET imaging at 20-min intervals at multiple time points before and after image-guided therapy. In this study, ^{15}O-water PET was evaluated as a tool to provide real-time feedback and iterative image guidance to rapidly monitor the intratumoral coverage of radiofrequency (RF) ablation therapy. **Methods:** Tumor RF ablation therapy was performed on head and neck squamous cell carcinoma (SCC) xenograft tumors (length, ~23 mm) in 6 nude rats. The tumor in each animal was ablated with RF (1-cm active size ablation catheter, 70°C for 5 min) twice in 2 separate tumor regions with a 20-min separation. The ^{15}O-water PET images were acquired before RF ablation and after the first RF and second RF ablations using a small-animal PET scanner. In each PET session, approximately 100 MBq of ^{15}O-water in 1.0 mL of saline were injected intravenously into each animal. List-mode PET images were acquired for 7 min starting 20 s before injection. PET images were reconstructed by 2-dimensional ordered-subset expectation maximization into single-frame images and dynamic images at 10 s/frame. PET images were displayed and analyzed with software. **Results:** Pre–RF ablation images demonstrate that ^{15}O-water accumulates in tumors with ^{15}O activity reaching peak levels immediately after administration. After RF ablation, the ablated region had almost zero activity, whereas the unablated tumor tissue continued to have a high ^{15}O-water accumulation. Using image feedback, the RF probe was repositioned to a tumor region with residual ^{15}O-water uptake and then ablated. The second RF ablation in this new region of the tumor resulted in additional ablation of the solid tumor, with a corresponding decrease in activity on the ^{15}O-water PET image. **Conclusion:** ^{15}O-water PET clearly demonstrated the ablated tumor region, whereas the unablated tumor continued to show high ^{15}O-water accumulation. ^{15}O-water imaging shows promise as a tool for on-site, real-time monitoring of image-guided interventional cancer therapy.

Image-guided interventional cancer therapy is an emerging local solid cancer therapy technique (1–3). With this cancer therapy technique, solid cancer is locally treated with thermal or cryoablation or with instillation of alcohol or chemotherapeutic agents.

Cancer thermal ablation with radiofrequency (RF), microwave, or focused ultrasound has been intensively investigated in experimental or human cancer therapy (4–8). Cancer thermal ablation provides a minimally invasive or noninvasive cancer therapy technique that rapidly kills cancer cells by heat. Cancer cell death is related to both the temperature and the time period of thermal exposure. However, tumor eradication relies on the complete thermal ablation of the whole tumor mass (6). After the initial thermal ablation, remaining viable tumor tissue may exist, and further thermal ablation is necessary to ensure complete delivery of the thermotherapy to the whole tumor. Accordingly, a rapid-feedback imaging technique would be useful for the real-time evaluation of thermal therapy coverage (8).

To assess the therapy coverage by thermal ablation, the use of contrast-enhanced CT, MRI, and ultrasound imaging has been investigated (9–15). In addition, MRI thermometry has been used in the real-time monitoring of the temperature distribution in the ablation site (16). An immediate effect of thermal ablation is the coagulation of tumor vasculature and the formation of a coagulation zone that covers either the whole tumor or a portion of the tumor (4). Because of the coagulation zone formation, blood-perfusion contrast agents may prove to be useful tools for the real-time monitoring of the coverage by thermal ablation (10).

In this article, we introduce the use of a perfusion radiotracer, ^{15}O-water, and PET imaging as a potential

technique for the real-time monitoring of thermal ablation. ^{15}O-water mostly represents the in vivo behavior of water after administration (17,18). The short, 2-min half-life of ^{15}O makes it practical to perform repeated PET scans at 20-min intervals at multiple time points before and after image-guided thermal therapy. In this study, ^{15}O-water PET was evaluated as a tool to provide real-time feedback and iterative image guidance to rapidly monitor the intratumoral coverage of RF ablation therapy of head and neck squamous cell carcinoma (SCC) xenografts in rats. A comparison between PET images and RF ablation coverage on the basis of the dissected tumors was also investigated.

MATERIALS AND METHODS

Animal Model

Animal studies were performed according to the National Institutes of Health animal use guidelines (19) and were approved by our Institutional Animal Care Committee. During animal-handling procedures, the animals were anesthetized with 1%–3% isoflurane (Vedco) in 100% oxygen using an anesthesia inhalation unit (Bickford). A head and neck SCC xenograft model in nude rats was set up by subcutaneously inoculating 5×10^6 human tongue SCC-4 cells (American Type Culture Collection) in 0.20 mL of saline into the back of the neck of each male *rnu/rnu* nude rat (Harlan) (age, 3–4 wk) at the scapula level. Tumor growth and histopathology for this cancer xenograft model have been previously characterized (20).
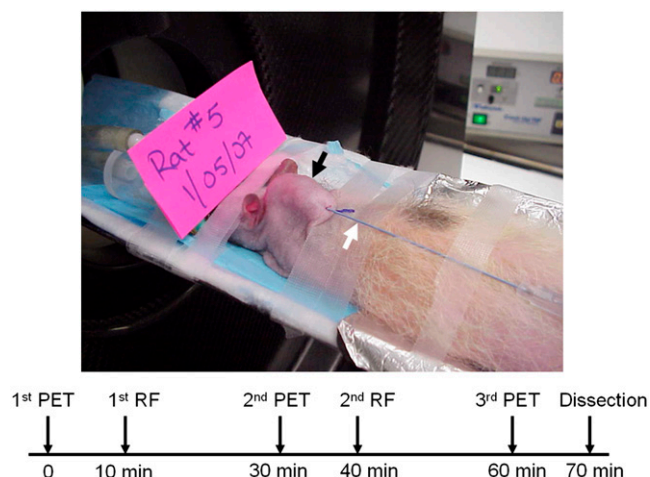
RF Ablation and ^{15}O-Water PET

Six male nude rats bearing SCC tumor xenografts were used for the studies. The RF ablation and ^{15}O-water PET studies were performed 16 d after tumor cell inoculation. On the day of the PET and RF ablation studies, the thickness, width, and length of each tumor were measured with a digital caliper, and the tumor volume was calculated using the equation V = thickness × width × length × π/6 (21). The average tumor dimensions were 11.74 (±2.67 [SD]) × 14.62 (±3.07) × 23.54 (±4.11) mm; the average tumor volume based on the calculation of caliper measurement was 2.16 ± 0.86 cm^3. The average body weight was 206.3 ± 11.7 g.

Immediately after placement of a 25-gauge needle catheter with 0.070 mL of dead volume into the tail vein of each rat under anesthesia, the rat was relocated onto the bed of the microPET R4 scanner (Siemens Medical Systems) and positioned to align the tumor of each animal in the center of the field of view in both axial and longitudinal directions. ^{15}O-water tracer in 1.0 mL of saline for injection (111.4 ± 36.3 MBq [3.01 ± 0.98 mCi]) prepared on site was injected approximately 20 s after the start of PET image acquisition. The injection procedure lasted around 10 s. Any remaining radioactivity in the catheter was not flushed from the catheter, to avoid variation and perturbation from the injection procedure. On the basis of the 70 μL of dead volume in the catheter, it was estimated that 7% of total activity was retained in the catheter and was not injected into the animal. Thus, the net ^{15}O activity injected was 103.6 ± 33.8 MBq (2.80 ± 0.91 mCi). Each PET image acquisition was collected in list mode for 7 min. After this baseline ^{15}O-water PET image acquisition, a 21-gauge RF ablation single straight-needle electrode (1-cm active element tip) was inserted into the caudal portion of the tumor, in parasagittal

orientation, to perform RF ablation using a protocol adapted from previous studies by Goldberg et al. (22) (Fig. 1). Because of the subcutaneous location of the tumor, the needle tip was easily placed in the center of the tumor by direct visualization and palpation. The caudal portion of the tumor was ablated for 5 min at 70°C using a 500-kHz RF generator (Cool-tip RF Ablation System; Valleylab Co.). To perform RF ablation, a standard ground electrode (Valleylab Co.) was enveloped in aluminum foil and placed in contact with the ventral surface of the animal, using electrolytic contact gel to ensure a large area of contact between animal and ground electrode. The RF ablation procedure used the manual-control mode of the generator to ensure that the ablation temperature was at 70°C, within 1°C variance.

Without repositioning of the RF electrical cathode, a second ^{15}O-water PET was performed within 20–30 min of the pre–RF ablation PET image acquisition, using the same ^{15}O-water injection and PET protocol as described for pre–RF ablation baseline imaging (average net ^{15}O activity injected, 104.8 ± 0.8 MBq [2.83 ± 0.02 mCi]). When the ^{15}O-water PET after the first RF ablation was completed, the RF ablation electrical cathode was repositioned to the cephalic portion of the tumor and in the same direction as the first RF ablation. A second RF ablation, with the same protocol as the first RF ablation and followed by ^{15}O-water PET within 20–30 min of the second ^{15}O-water injection, was performed (average net ^{15}O activity injected, 105.5 ± 0.14 MBq [2.85 ± 0.004 mCi]).

After completion of the RF ablation and ^{15}O-water PET, each animal was euthanized via cervical dislocation under deep anesthesia sedation. The tumor in each animal was dissected and cut along the insertion pathway of the RF ablation electrical cathode. The tumor sections were fixed with 10% buffered formalin (Fisher Scientific). The formalin-fixed tumor samples were then sectioned, placed in cassettes, processed, and embedded in paraffin. Five-micrometer-thick sections of each specimen were prepared and stained with hematoxylin and eosin (H&E) by the Department of Pathology Core Laboratory of our university, using standard

FIGURE 1. Experimental setup for real-time monitoring of RF ablation with ^{15}O-water PET. RF ablation catheter (white arrow) was inserted into tumor xenograft located on back of rat's neck (black arrow). Ground electrode covered in aluminum foil was placed underneath rat. Flow chart indicates approximate times from 0 to 70 min and sequence for performing ^{15}O-water PET, RF ablation, and tumor dissection of each animal.

procedures. H&E slides were scanned at low resolution using a high-resolution laser scanner or observed with a microscope (BH-2; Olympus) equipped with a digital camera (PowerShot S3 IS; Canon) under low and high magnification.

Image Analysis

A global decay correction using the half-life of 122.24 s was applied to the dataset. The PET images were reconstructed by 2-dimensional ordered-subset expectation maximization into single-frame images and dynamic images at 10 s/frame with small-animal PET manager software (Concorde MicroSystems) (matrix size, 128 × 128 × 63; voxel size, 0.85 × 0.85 mm; slice thickness, 1.20 mm). The PET images were displayed and analyzed with software (ASIPro; Concorde MicroSystems).

Time–Activity Curves from Region-of-Interest (ROI) Analysis of Dynamic ^{15}O-Water PET Images

The average relative pixel values of each tumor on the pre–RF ablation images and the first and second RF ablation images were analyzed by manually placing ROIs (8–12 pixels with each ROI) on the central region (ablated region) and the rim of each tumor (unablated region) of the coronal slice. The largest ablated area is shown in Figures 2 and 3. The average pixel values and their SDs of tumors of all 6 rats at each time point were calculated with Excel software (Microsoft). The graphs of dynamic average values in the ROI with time were plotted and formatted using software (Origin, version 7.5; Origin Lab).

3-Dimensional ROI Analysis of Ablated Region

The total pixel number (n) of the ablated region, resulting from the first and second RF ablations in each tumor in each PET image, was calculated by manually drawing a 3-dimensional ROI around the entire tumor and around the ablated central region of the tumor. The RF-ablated region was determined by defining the edge using a threshold-based method (23). Profile analysis revealed a transition zone of about 2–3 pixels from very low activity between ablated and unablated regions before an unablated high-activity plateau was reached. As shown in Figures 2 and 3, the RF ablation ROI represents the area with pixel values of less than 30% of the maximum pixel value in each slice of the 3-dimensional tumor volume, and the ROI was drawn to include the regions below the 30% threshold value without partial-volume

correction. The volumes of ablated regions resulting from the RF ablations were calculated with the following equation:

$$V(cm^3) = n \times 0.85 \times 0.85 \times 1.2/1,000.$$

The comparison between PET images and dissected tumors used the method of drawing a region of RF-ablated tissue and comparing it to the ablated region in PET images in the tumor slice.

Statistical Analysis

Statistical analyses used Origin software. The comparison between the ablated region volumes after the first and second RF ablations was analyzed by paired t test under the hypothesis that the volume after the second RF ablation was larger than that after the first RF ablation. The statistical analysis of the comparison on the relative values of ablated and unablated regions of the tumor at each time point with each PET image used paired t testing under the hypothesis that each set of values was not equal. A value of P less than 0.05 was considered significantly different.
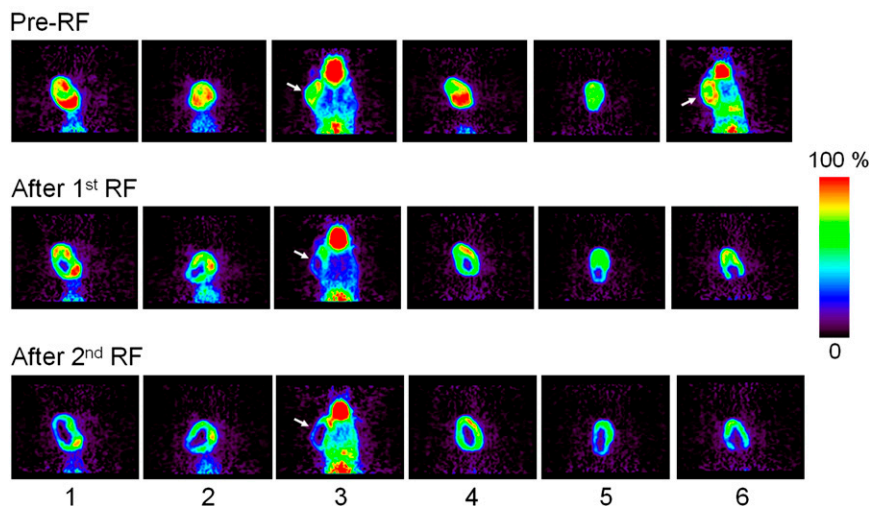
RESULTS
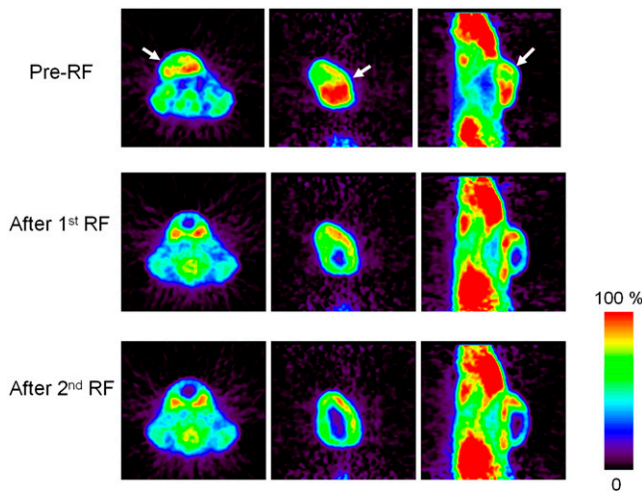
^{15}O-Water PET

The coronal images of all 6 rats bearing head and neck SCC tumors before RF ablation and after the first and second RF ablations are shown in Figure 2.

Pre–RF Ablation Image Analysis

The images in Figures 2 and 3 demonstrate that ^{15}O-water accumulated readily in tumors, and the tumor margin had higher radioactivity than did the tumor center. Analysis of the average pixel value within the tumor from the dynamic images with 10 s/frame showed that the tumor margin (higher-activity unablated region) reached a peak of ^{15}O activity within 20 s after ^{15}O-water administration, followed by a gradual clearance during the 7-min time period (Fig. 4A). Comparably, the tumor center (ablated region) had a lower activity per unit volume ($P < 0.01$ at 30 s) than did the tumor margin and a gradual increase in ^{15}O activity during

FIGURE 2. ^{15}O-water PET images of all 6 rats bearing head and neck SCC xenografts (coronal images) at time points of before RF ablation, after first RF ablation, and after second RF ablation. Image slices are mainly focused on tumors located in center of neck for rats 1, 2, 4, and 5 or slightly on side of neck for rats 3 and 6 (arrows). Because of motility of subcutaneous tumor xenograft, geometry of tumor in rat 6 was different before and after each RF ablation.

FIGURE 3. Representative ^{15}O-water PET images of rat bearing head and neck SCC xenograft (left, axial images; middle, coronal images; right, sagittal images) at time points of before RF ablation, after first RF ablation, and after second RF ablation. Arrows point to tumor.

the 7-min time period (Fig. 4A). By the end of the 7-min ^{15}O-water PET period, tumor margin and tumor center reached similar ^{15}O activity levels.

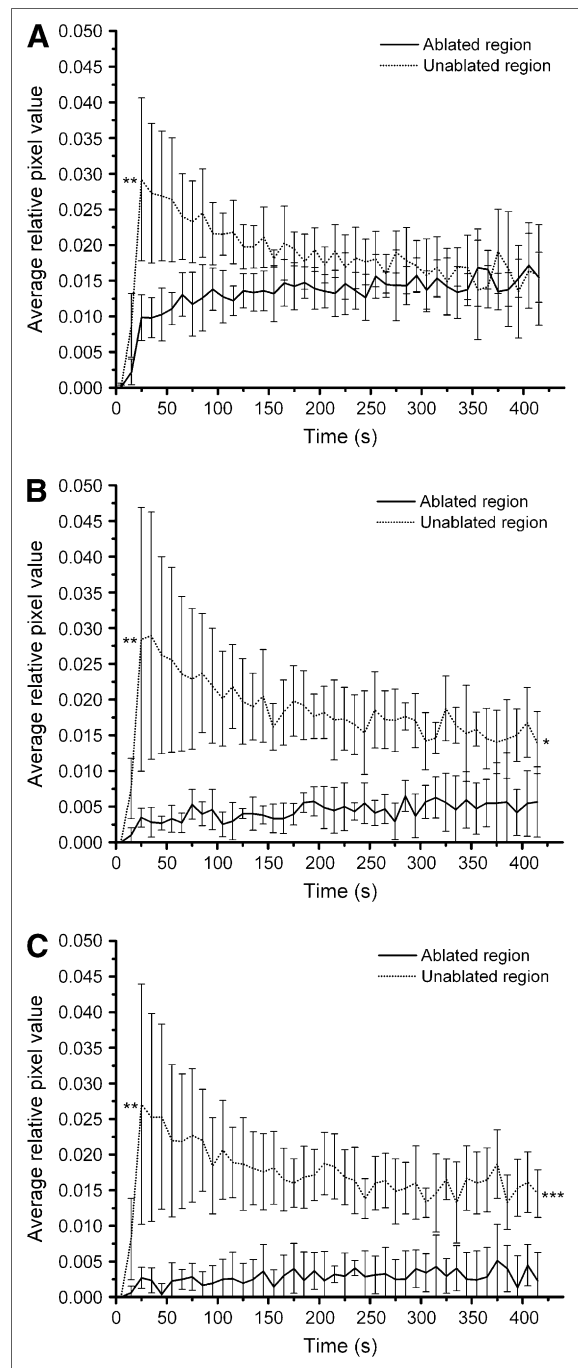**Post–RF Ablation Image Analysis**

The first RF ablation resulted in an area in the caudal region of each tumor with decreased ^{15}O activity (Figs. 2 and 3). The second RF ablation further expanded the low-activity ablated region in the cephalic portion of the tumor. Analysis of the dynamic images demonstrates that the RF-treated region in the tumor had minimal ^{15}O activity (Figs. 4B and 4C). The tumor margin had an ^{15}O activity accumulation profile that was similar to the activity in the tumor center before RF ablation. These results demonstrate an immediate decrease in ^{15}O-water accumulation after RF ablation. The volume of ablated region after the first RF ablation was 0.41 ± 0.22 cm^3, whereas the volume of ablated region after the second RF ablation was 0.94 ± 0.23 cm^3. The ablated region volume after second RF ablation was significantly larger than it was after first RF ablation ($P = 0.001$).

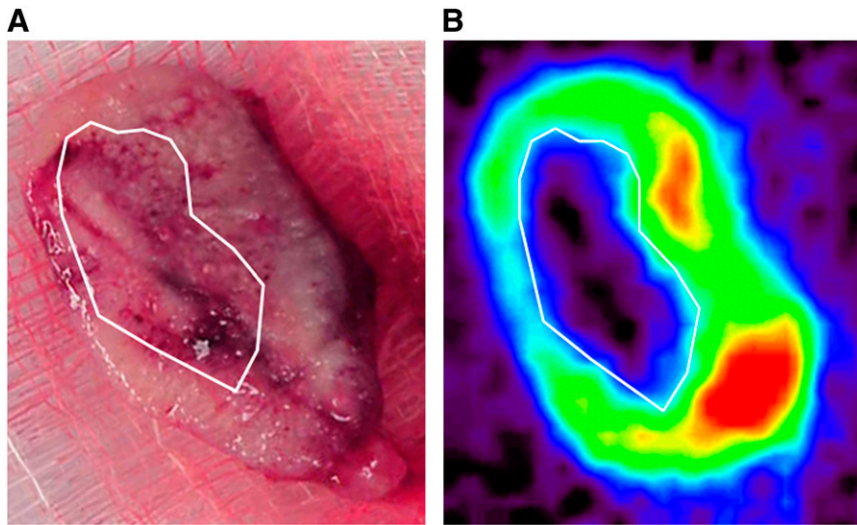**Similar Pattern of Tissue RF Ablation Region and ^{15}O-Water Distribution**

On gross pathologic examination of the dissected tumors, there was an observable pattern of blood infiltration of the tumor tissue after the RF ablation that matched the pattern on the ^{15}O-water PET image (Fig. 5). The lower-activity ablated region of ^{15}O-water distribution in PET images and RF ablation coverage as shown by the coagulation zones in freshly dissected tumors had a similar distribution (Figs. 5A and 5B). Tissue RF ablation regions and the ablated regions depicted on the PET image had the same shape and size.

The H&E-stained section demonstrated that the difference between the RF-ablated and the non–RF-ablated

FIGURE 4. Relative pixel-value (average $\pm$ SD) time curves determined by ROI analysis of dynamic ^{15}O-water PET images with 10 s/frame before and after RF ablation of tumors ($n = 6$). For pre–RF ablation analysis (A), ablated region represents ROI drawn in tumor center, whereas unablated region represents ROI drawn at tumor margin. For first RF ablation (B) and second RF ablation (C), ablated region represents area in tumor center after RF ablation and unablated region represents area in tumor margin that was not ablated (*$P < 0.05$, **$P < 0.01$, and ***$P < 0.001$ compare ablated and unablated regions at same time points).

FIGURE 5. Comparison between coagulation zone shown in freshly dissected tumor (A) and ablated region in ^{15}O-water PET image (B). Coagulation zone (marked area) has similar shape and size corresponding to ablated region in ^{15}O-water PET image.

regions in a tumor was mainly because of coagulative necrosis, blood coagulation, and blood infiltration into the tumor interstitial space in the RF-ablated region (Fig. 6), which is normally observed after thermal ablation (*4*). Under higher magnification, RF-ablated tumor tissue, compared with nonablated tissue, also had enlarged cell nuclei (data not shown). In addition, decreased tumor tissue integrity in the RF-ablated region, with a decreased adherence among cells and between tumor cells and their extracellular matrix, which is indicated by the loss of cells in RF-ablated tissue region on the H&E-stained sections (Fig. 6), was observed.
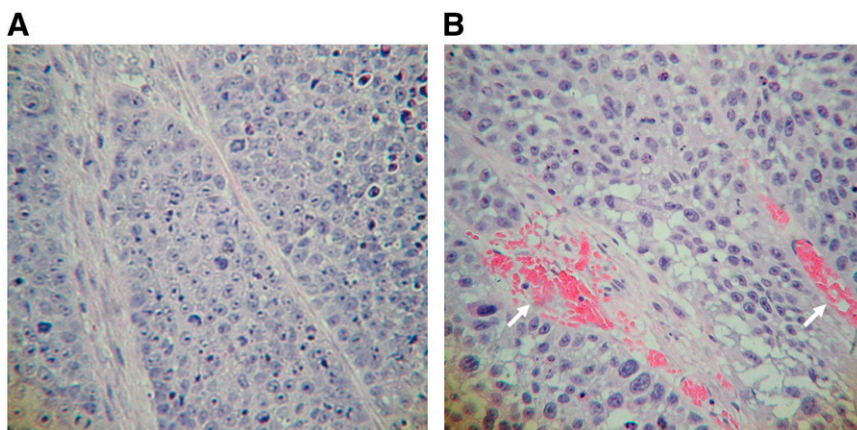
DISCUSSION

This study demonstrates the potential use of ^{15}O-water PET for real-time monitoring of image-guided tumor thermal therapy. The region of the RF ablation was clearly demonstrated, with a rapid feedback in fewer than 20 min. ^{15}O-water can be used repeatedly during the same therapy session because of its short, 2-min physical half-life and associated low–radiation-absorbed dose. Injection of ^{15}O-water as an imaging agent is also extremely safe and has almost no possibility of causing a contrast-related adverse reaction.

Prior clinical studies with ^{15}O-water have also demonstrated that liver tumors can be imaged with ^{15}O-water for the monitoring of chemotherapy (*24*). To monitor liver tumor therapy by RF ablation, ^{18}F-FDG PET and other imaging methods have been investigated (*25,26*). It has been shown that ^{18}F-FDG imaging may be useful for assessment of the effectiveness of tumor RF ablation. However, these studies did not use real-time assessment of the coverage of tumor RF ablation, which was made possible in this study because of the short half-life of ^{15}O.

One of the strengths of ^{15}O-water PET is its ability to directly monitor the physiologic process of blood flow, which is generally increased in solid tumors along with tumor metabolism. In our studies, the blood flow to the tumor margin was significantly greater than that to the central portion of the tumor. It is the tumor margin, with its increased blood flow, that is most difficult to treat with thermal ablation because of heat dissipation from increased blood flow. Therefore, in clinical thermal RF ablation tumor

FIGURE 6. H&E-stained tumor section that was not RF ablated (A) and was RF ablated (B) (20× magnification for both tumor sections). Red color component (arrows) in RF-ablated tumor tissue is because of coagulated and infiltrated blood cells.

regrowth generally occurs at the margins of the tumor. Previous histopathologic characterization of the tumor model used in this study revealed surviving tumor cells throughout the whole tumor section, including both the tumor margin and the tumor center, although a greater number of necrotic tumor cells were evident in the tumor center (*20*). The extracellular matrix–supported tumor blood vessels were located in the whole tumor section from the tumor margin to the tumor center; however, the tumor margin had a more abundant blood vessel supply, including larger blood vessels at the tumor surface.

In RF ablation planning, the goal of the RF ablation treatment is to not only ablate the tumor but also ablate a 1-cm margin of normal tissue surrounding the tumor (*6*). Historically, it has been difficult to create ablations that are much larger than 3 cm in diameter with RF ablation single straight-needle electrodes (*27*), which are commonly used in clinical practice. Recent technical advancements using perfusion or bipolar or multipolar electrodes can allow the ablation area to reach over 5 cm in diameter (*28–33*).

To ensure the eradication of the entire tumor, real-time image monitoring is necessary, due to the possibility of an unpredictable ablation volume in a particular patient associated with difficulty in accurately knowing the area of tumor and surrounding normal tissue treated with each ablation. ^{15}O-water imaging with rapid feedback of ablated volumes and repeated iterative thermal ablation and re-imaging with ^{15}O-water offers the possibility of improving thermal therapy and ensuring that the margin of the tumor has been adequately treated. In clinical practice, the PET image would most likely be fused with a simultaneously acquired CT image, and the CT image would be used to provide real-time image guidance for placement of the RF ablation probe.

Another promising approach being investigated to improve solid tumor thermal therapy is MRI thermometry monitoring (*16*). This technique offers the possibility of precisely determining the elevation of temperature to the tumor and regions surrounding the tumor. An advantage of the ^{15}O-water imaging technique is that it directly monitors the tumor physiologic change in relationship to the coagulation of the tumor caused by the thermal ablation. Contrast-enhanced MRI has also been investigated for the real-time monitoring of thermal ablation (*10,11,13*). Although MRI contrast agents, such as Gd-diethylenetriaminepentaacetic acid, may be useful for monitoring thermal ablation, their kinetics of tumor accumulation after RF ablation could be different from ^{15}O-water because of their decreased ability to penetrate through blood vessels into the tumor interstitial space. In addition, contrast-enhanced ultrasound may be useful for the real-time image monitoring of thermal ablation (*9,14,15*). Further investigation of comparative studies of these imaging modalities for real-time monitoring of RF ablation would be worthwhile.

One obvious concern of this technique is the requirement that imaging and therapy need to be performed near a cyclotron capable of ^{15}O production. However, dedicated cyclotrons for producing ^{15}O can be manufactured at a much lower cost than higher-energy cyclotrons for production of other PET radionuclides. Cyclotrons associated with academic medical centers have also become more widely available.

CONCLUSION

The feasibility of using ^{15}O-water PET for on-site real-time monitoring of image-guided interventional cancer therapy is demonstrated in this preclinical animal model.

REFERENCES

1. Hong K, Georgiades CS, Geschwind J-FH. Technology insight: image-guided therapies for hepatocellular carcinoma—intra-arterial and ablative techniques. *Nature Clin Practice Oncol.* 2006;3:315–324.
2. Dodd GD, Soulen MC, Kane RA, et al. Minimally invasive treatment of malignant hepatic tumors: at the threshold of a major breakthrough. *Radiographics.* 2000;20:9–27.
3. Gedroyc WMW. Magnetic resonance guidance of thermal ablation. *Top Magn Reson Imaging.* 2005;16:339–353.
4. Haemmerich D, Laeseke PF. Thermal tumour ablation: devices, clinical applications and future directions. *Int J Hyperthermia.* 2005;21:755–760.
5. Kurumi Y, Tani T, Naka S, et al. MR-guided microwave ablation for malignancies. *Int J Clin Oncol.* 2007;12:85–93.
6. Dodd GD, Frank M, Aribandi M, Chopra S, Chintapalli KN. Radiofrequency thermal ablation: computer analysis of the size of the thermal injury created by overlapping ablations. *AJR.* 2001;177:777–782.
7. Haar GT, Coussios C. High intensity focused ultrasound: physical principles and devices. *Int J Hyperthermia.* 2007;23:89–104.
8. Bland KL, Gass J, Klimberg VS. Radiofrequency, cryoablation, and other modalities for breast cancer ablation. *Surg Clin North Am.* 2007;87:539–550.
9. Lu MD, Yu XL, Li AH, et al. Comparison of contrast enhanced ultrasound and contrast enhanced CT or MRI in monitoring percutaneous thermal ablation procedure in patients with hepatocellular carcinoma: a multi-center study in China. *Ultrasound Med Biol.* 2007;33:1736–1749.
10. Cheng H-LM, Purcell CM, Bilbao JM, Plewes DB. Prediction of subtle thermal histopathological change using a novel analysis of Gd-DTPA kinetics. *J Magn Reson Imaging.* 2003;18:585–598.
11. Bathe OF, Mahallati H. MR-guided ablation of hepatocellular carcinoma aided by gadoxetic acid. *J Surg Oncol.* 2007;95:670–673.
12. Johnson DB, Duchene DA, Taylor GD, Pearle MS, Cadeddu JA. Contrast-enhanced ultrasound evaluation of radiofrequency ablation of the kidney: reliable imaging of the thermolesion. *J Endourol.* 2005;19:248–252.
13. Clasen S, Boss A, Schmidt D, et al. Magnetic resonance imaging for hepatic radiofrequency ablation. *Eur J Radiol.* 2006;59:140–148.
14. Slabaugh TK Jr, Machaidze Z, Hennigar R, Ogan K. Monitoring radiofrequency renal lesions in real time using contrast-enhanced ultrasonography: a porcine model. *J Endourol.* 2005;19:579–583.
15. Solbiati L, Tonolini M, Cova L. Monitoring RF ablation. *Eur Radiol.* 2004;14(suppl 8):P34–P42.
16. De Senneville BD, Mougenot C, Quesson B, Dragonu I, Grenier N, Moonen CT. MR thermometry for monitoring tumor ablation. *Eur Radiol.* 2007;17:2401–2410.
17. Lodge MA, Carson RE, Carrasquillo JA, Whatley M, Libutti SK, Bacharach SL. Parametric images of blood flow in oncology PET studies using [^{15}O]water. *J Nucl Med.* 2000;41:1784–1792.

18. Ludemann L, Sreenivasa G, Michel R, et al. Corrections of arterial input function for dynamic $H_2^{15}O$ PET to assess perfusion of pelvic tumours: arterial blood sampling versus image extraction. *Phys Med Biol.* 2006;51:2883–2900.

19. *Guide for the Care and Use of Laboratory Animals.* Washington, DC: National Academy Press; 1996.

20. Bao A, Phillips WT, Goins B, et al. Setup and characterization of a human head and neck squamous cell carcinoma xenograft model in nude rats. *Otolaryngol Head Neck Surg.* 2006;135:853–857.

21. Tomayko MM, Reynolds CP. Determination of subcutaneous tumor size in athymic (nude) mice. *Cancer Chemother Pharmacol.* 1989;24:148–154.

22. Goldberg SN, Kruskal JB, Oliver BS, Clouse ME, Gazelle GS. Percutaneous tumor ablation: increased coagulation by combining radio-frequency ablation and ethanol instillation in a rat breast tumor model. *Radiology.* 2000;217:827–831.

23. Drever L, Roa W, McEwan A, Robinson D. Comparison of three image segmentation techniques for target volume delineation in positron emission tomography. *J Appl Clin Med Phys.* 2007;8:93–109.

24. Koh T, Taniguchi H, Yamagishi H. Oxygen-15 positron-emission tomography for predicting selective delivery of a chemotherapeutic agent to hepatic cancers during angiotensin II-induced hypertension. *Cancer Chemother Pharmacol.* 2003;51:349–358.

25. Antoch G, Vogt FM, Veit P, et al. Assessment of liver tissue after radiofrequency ablation: findings with different imaging procedures. *J Nucl Med.* 2005;46:520–525.

26. Yamagami T, Kato T, Tanaka O, Hirota T, Nishimura T. Radiofrequency ablation therapy of remnant colorectal liver metastases after a course of hepatic arterial infusion chemotherapy. *J Vasc Interv Radiol.* 2005;16:549–554.

27. Livraghi T, Goldberg SN, Lazzaroni S, et al. Hepatocellular carcinoma: radio-frequency ablation of medium and large lesions. *Radiology.* 2000;214:761–768.

28. Seror O, N'Kontchou G, Ibraheem M, et al. Large (≥5.0-cm) HCCs: multipolar RF ablation with three internally cooled biopolar electrodes—initial experience in 26 patients. *Radiology.* 2008;248:288–296.

29. Goldberg SN. Radiofrequency tumor ablation: principles and techniques. *Eur J Ultrasound.* 2001;13:129–147.

30. Terraz S, Constantin C, Majno PE, Spahr L, Mentha G, Becker CD. Image-guided multipolar radiofrequency ablation of tumours: initial clinical results. *Eur Radiol.* 2007;17:2253–2261.

31. Kim SK, Myung SG, Hong HP, Choi D, Chae SW. CT findings after radiofrequency ablation in rabbit livers: comparison of internally cooled electrodes, perfusion electrodes, and internally cooled perfusion electrodes. *J Vasc Interv Radiol.* 2007;18:1417–1427.

32. Pereira PL, Trübenbach J, Schenk M, et al. Radiofrequency ablation: in vivo comparison of four commercially available in pig livers. *Radiology.* 2004;232:482–490.

33. Navarro AC, Burdío F, Berjano EJ, et al. Small ablation zones created previous to saline infusion result in enlargement of the coagulated area during perfusion RF ablation: an *ex vivo* experimental study. *Physiol Meas.* 2007;28:N29–N37.